RESEARCH ARTICLE

NANO · MICRO small
www.small-journal.com

Lipid Monolayer on Cell Surface Protein Templates Functional Extracellular Lipid Assembly

*Anupma Dwivedi, Anisha Mazumder, Petra Pullmannová, Anna Paraskevopoulou, Lukáš Opálka, Andrej Kováčik, Miloslav Macháček, Pavla Jančálková, Petra Svačinová, Herwig Peterlik, Jaroslav Maixner, and Kateřina Vávrová**

When the ancestors of men moved from aquatic habitats to the drylands, their evolutionary strategy to restrict water loss is to seal the skin surface with lipids. It is unknown how these rigid ceramide-dominated lipids with densely packed chains squeeze through narrow extracellular spaces and how they assemble into their complex multilamellar architecture. Here it is shown that the human corneocyte lipid envelope, a monolayer of ultralong covalently bound lipids on the cell surface protein, templates the functional barrier assembly by partly fluidizing and rearranging the free extracellular lipids in its vicinity during the sculpting of a functional skin lipid barrier. The lipid envelope also maintains the fluidity of the extracellular lipids during mechanical stress. This local lipid fluidization does not compromise the permeability barrier. The results provide new testable hypotheses about epidermal homeostasis and the pathophysiology underlying diseases with impaired lipid binding to corneocytes, such as congenital ichthyosis. In a broader sense, this lipoprotein-mediated fluidization of rigid (sphingo)lipid patches may also be relevant to lipid rafts and cellular signaling events and inspire new functional materials.

1. Introduction

During cornification (keratinization), the specialized cell death in the epidermis,[1] the cells extrude abundant lipid aggregates and process them into a multilamellar, ceramide-dominated extracellular matrix in the uppermost skin layer, the stratum corneum[2] (SC; **Figure 1a–e**). These lipids are our first line of defense against various environmental threats,[3] so it is not surprising that they have predominantly densely packed, very long to ultralong saturated chains.[4–6] Indeed, the fluidization of these tightly packed lipid chains has been recognized as a permeation-enhancing strategy for transdermal and topical drug delivery.[7]

However, it is less conceivable how such rigid lipids attain their complex extracellular architecture, characterized by an ≈11–13 nm periodic lamellar arrangement, the long periodicity phase (LPP).[8,9] The skin barrier lipids are not transported to the extracellular space as individual molecules but pre-ordered lipid aggregates are released from granulocytes and, after enzymatic processing, must be very efficiently and precisely assembled into a multilamellar "mortar" that completely fills the space between the corneocytes in the mature barrier.[9,10] During the lipid extrusion and processing at the stratum granulosum/SC interface (Figure 1d),

A. Dwivedi, A. Mazumder, P. Pullmannová, A. Paraskevopoulou, L. Opálka, A. Kováčik, P. Jančálková, K. Vávrová
Skin Barrier Research Group, Faculty of Pharmacy
Charles University
Heyrovského 1203, Hradec Králové 50005, Czech Republic
E-mail: katerina.vavrova@faf.cuni.cz

A. Paraskevopoulou, A. Kováčik, P. Svačinová
Department of Pharmaceutical Technology, Faculty of Pharmacy
Charles University
Heyrovského 1203, Hradec Králové 50005, Czech Republic

M. Macháček
Department of Biochemical Sciences, Faculty of Pharmacy
Charles University
Heyrovského 1203, Hradec Králové 50005, Czech Republic

H. Peterlik
Faculty of Physics
University of Vienna
Boltzmanngasse 5, Vienna 1090, Austria

J. Maixner
Faculty of Chemical Technology
University of Chemistry and Technology Prague
Technická 5, Prague 16628, Czech Republic

The ORCID identification number(s) for the author(s) of this article can be found under https://doi.org/10.1002/smll.202307793

DOI: 10.1002/smll.202307793

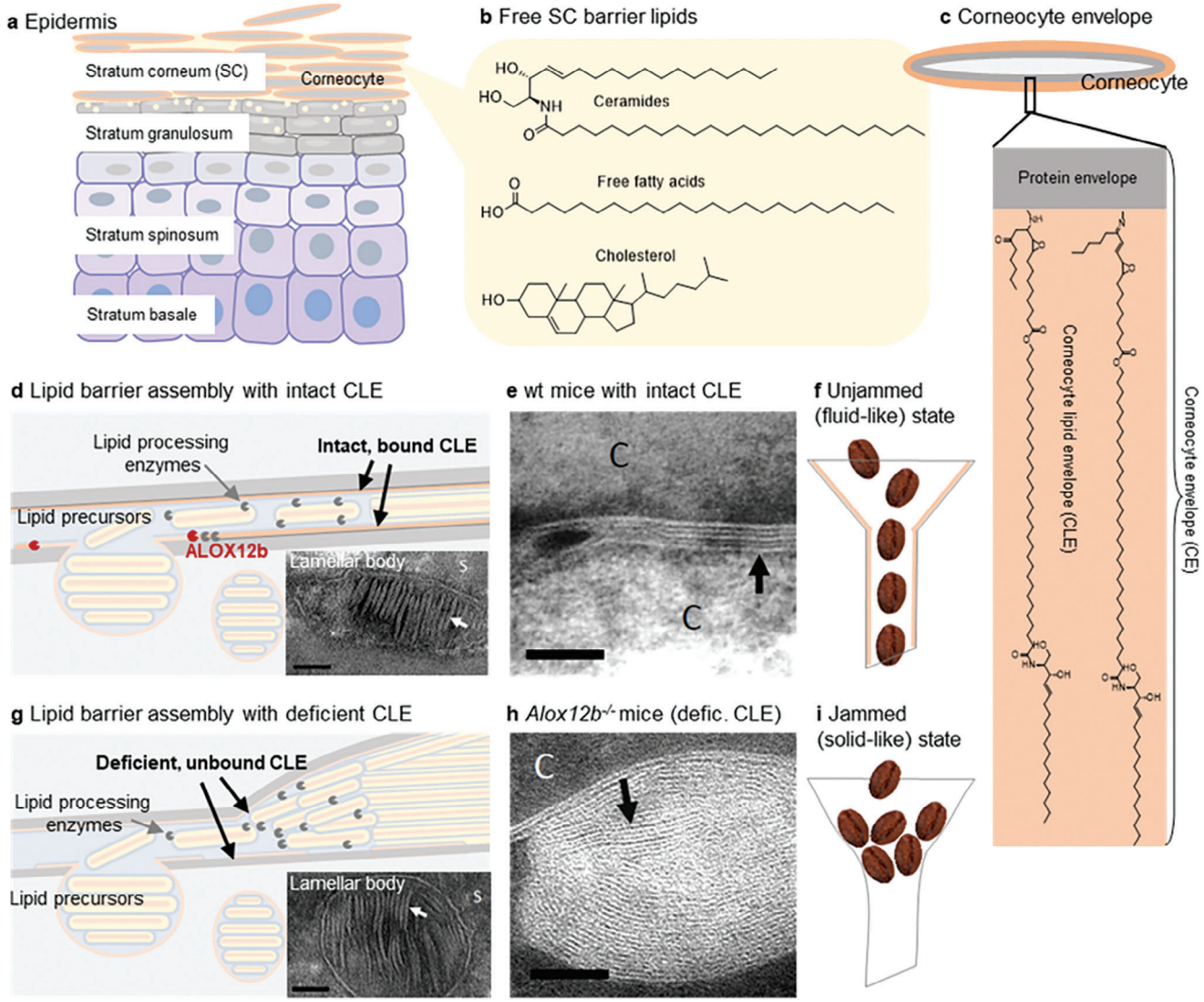

Figure 1. Formation of the skin lipid barrier and the proposed role of the corneocyte lipid envelope (CLE). a) Cartoon of the epidermis, with its uppermost layer, stratum corneum (SC), where the major permeability barrier is located. b) The extracellular SC lipids comprise mainly ceramides, free fatty acids, and cholesterol. c) Corneocytes have a corneocyte envelope (CE), composed of a cross-linked protein envelope with a covalently attached lipid monolayer, the CLE. d) The SC extracellular lipids are derived from lamellar bodies and require intact CLE for proper assembly and function (e). g) In diseases with compromised CLE, lipid assembly is impaired, for example in *Alox12b*$^{-/-}$ mice (h). Panels f) and i) show cartoons of unjammed state (mobile, fluid-like) and jammed state (solid-like, immobile), respectively. Ultrastructural images e) and h) are reproduced with permission from Ref. [18] (2023, Elsevier). Scale bar = 100 nm, arrow indicates lipid lamellae; C – corneocyte.

high-resolution cryo-electron microscopy has identified several distinct lamellar patterns,[11] suggesting dynamic lipid remodeling of the extracellular lipid matrix. Such remodeling requires a degree of the malleability of its components, i.e., a transient departure of lipid aggregates from solid-like to fluid-like behavior, which would be consistent with a hallmark of unjamming transitions in developmental dynamics.[12] Such an unjamming transition from a rigid solid-like to a flowing fluid-like matter has been recognized in various nonliving materials (e.g., a pile of sand or coffee beans in a chute) and living cells[13] (e.g., during morphogenesis,[14,15] wound healing,[16] and cancer[17]).

Unlike unjammed grains of sand or coffee beans (Figure 1f,i), which flow but are still solid at a molecular level, tissue unjamming involves cell rearrangement, effectively "melting" the tissue locally.[15] Thus, local (partial) fluidization of SC lipid aggregates may be a critical step in skin barrier remodeling. But what makes the predominantly rigid skin lipids with high transition temperatures fluid enough to rapidly squeeze into and fill narrow extracellular spaces without significant packing defects? Recent studies have identified an unexpectedly dynamic behavior of the sphingosine chains in ceramide, in contrast to their rigid *N*-acyl moieties.[19] Furthermore, linoleate chain ester-bound in ultralong *ω*-*O*-acylceramide

species (≈2–3 mol% of skin lipids) is isotropic.[20–22] However, although isolated human SC lipids in vitro are able to assemble into a proper lamellar structure, LPP, they require additional fluidization to reduce nanoscopic packing defects and permeability.[23]

We hypothesized that the corneocyte lipid envelope, CLE (Figure 1c), a lipid monolayer coating the corneocyte surface,[1,24] may template and locally fluidize the extracellular lipids. This lipid coat, rich in ultralong *ω-O*-acylceramides, is covalently anchored to a highly cross-linked protein envelope on the cell surface, together forming the corneocyte envelope (CE).[1] The essential nature of CLE in skin barrier homeostasis has been documented in several lipids–synthetic ichthyoses converging on CLE,[25] but its function remains unknown. Our hypothesis contrasts with the current view of the CLE as a brush-like scaffold driving the tight extracellular lipid packing.[10,25,26] One of the most compelling examples supporting our hypothesis is the lipid ultrastructure in *Alox12b*$^{-/-}$ mice (Figure 1g,h). These mice lack the 12R-lipoxygenase necessary for CLE binding to the cell surface, and although they have normal free extracellular lipids, their barrier function is impaired (≈twofold higher water loss). The lack of bound CLE in *Alox12b*$^{-/-}$ mice slows lipid maturation into the LPP triplet pattern, alters lamellar architecture, and impedes lipid assembly in extracellular spaces, which become significantly thicker with ≈threefold more lipid lamellae compared to wild-type mice.[18] These data suggest that in the absence of CLE, the energy barrier is too high to allow proper diffusion and rearrangement of extracellular lipids.

Here we study the interactions of free extracellular human SC lipids with isolated human CEs with or without intact CLE using biophysical and permeability experiments. We report that the CLE lipids template, fluidize and rearrange the free barrier lipids in their vicinity, for the first time suggesting an unjamming transition in the skin permeability barrier development.

2. Results and Discussion

2.1. CLEs Have Remarkably Disordered Lipid Chains Compared to Free SC Lipids

To examine the interactions of the CLE with the free extracellular skin barrier lipids, we isolated CEs (containing both the protein envelope and CLE) and extractable lipids from the human SC. The free SC lipids contained ceramides, free fatty acids, and cholesterol in approximately equimolar proportions and ≈2 mol% cholesteryl sulfate, as shown by high-performance thin layer chromatography (HPTLC). The ceramide fraction was further quantified by liquid chromatography coupled to tandem mass spectrometry (LC-MS^2), and the percentages of the 16 most abundant ceramide subclasses, including their acyl chain lengths, together with the chemical structures of these sphingolipids, are shown in Figure S1 (Supporting Information). This composition is consistent with that of human SC.[9] The CEs are routinely obtained by boiling the tissue in an extraction buffer containing sodium dodecyl sulfate (SDS).[27] We found traces of SDS by infrared spectroscopy (detected as CD_2 bands when using deuterated SDS, Figure S2a–d, Supporting Information) in the CE samples even after extensive purification and washing, likely because of the SDS hydrophobicity and negative charge. Strong SDS binding has been described for a number of membrane-associated proteins during SDS-PAGE.[28] We therefore modified the method by using *N,N*-dimethyldodecylamine *N*-oxide (DDAO), a neutral surfactant. The isolated CEs stained positive for the surface protein involucrin and lipids (**Figure 2a**), in agreement with the literature.[27] Infrared spectroscopy revealed that the CLE chains were remarkably disordered, as indicated by the methylene symmetric stretching wavenumbers of 2852.4 ± 0.2 cm^{-1}, in contrast to the well-ordered lipid chains in the untreated SC (2848.8 ± 0.3 cm^{-1}; a lower wavenumber indicates more ordered chains; Figure 2b). This difference is quite large; for comparison, the values found in vivo in patients with atopic dermatitis and healthy volunteers were 2849.2 and 2848.8 cm^{-1}, respectively (the difference was significant and related to functional barrier impairment).[29] Notably, in SDS-isolated samples, the CLE chains were less fluid (2850.6 ± 0.1 cm^{-1}), probably due to residual SDS incorporated between them (Figure S2c, Supporting Information). It should be noted that CLE properties may be further modulated by cellular proteins (we focused here on the envelopes to obtain reproducible data, as our pilot experiments with shorter extraction procedures resulted in corneocytes with varying protein content). Nevertheless, disordered lipid chains were also observed in solvent-extracted SC with the cellular proteins (2852.2 ± 0.9 cm^{-1}; Figure 2b), confirming that this property is not an artifact of CE isolation. Such fluid CLE can be explained by the anchoring of lipids in the CEs at relatively low grafting density. This assumption corresponds to the reported average CE mass per area[30] of 7 kDa nm^{-2}, which roughly gives the lipid density of ≈700 Da nm^{-2} (assuming a protein-to-lipid ratio of 9:1 in the CE[31]). This estimate gives approximately one lipid chain per nm^2, an area that could accommodate five fully stretched chains. Such a low lipid density is consistent with the origin of the lipid envelope from the coating membrane of the lamellar body, which is rich in phospholipids that are eventually hydrolyzed during cornification.

We also isolated saponified CEs (sapCEs). The tissue was first saponified to remove the covalent lipids from the surface proteins; the individual sapCEs were obtained using the above procedure, although with lower yields due to their fragility. The sapCEs also stained positive for involucrin and, somewhat surprisingly, with Nile Red (Figure S2e, Supporting Information). In contrast, corneocytes isolated from the epidermis without bound lipid envelopes (such as in PNPLA1 deficiency) do not stain with Nile Red because such CEs are not hydrophobic.[27] Such staining, which did not disappear after extensive washing, indicates that hydrophobic material is retained on the CE surface. This result favors the recently proposed direct attachment of the epoxy enone form of *ω-O*-acylceramides to involucrin[32] over the previously proposed hydrolysis of oxidized *ω-O*-acylceramides followed by the *ω*-hydroxyceramide attachment via terminal hydroxyl.[33] In the first case, linoleic acid residues would remain on the corneocyte surface after ester saponification, consistent with Nile Red staining. In the latter case, no significant hydrophobic material would remain on the corneocyte surface after saponification.

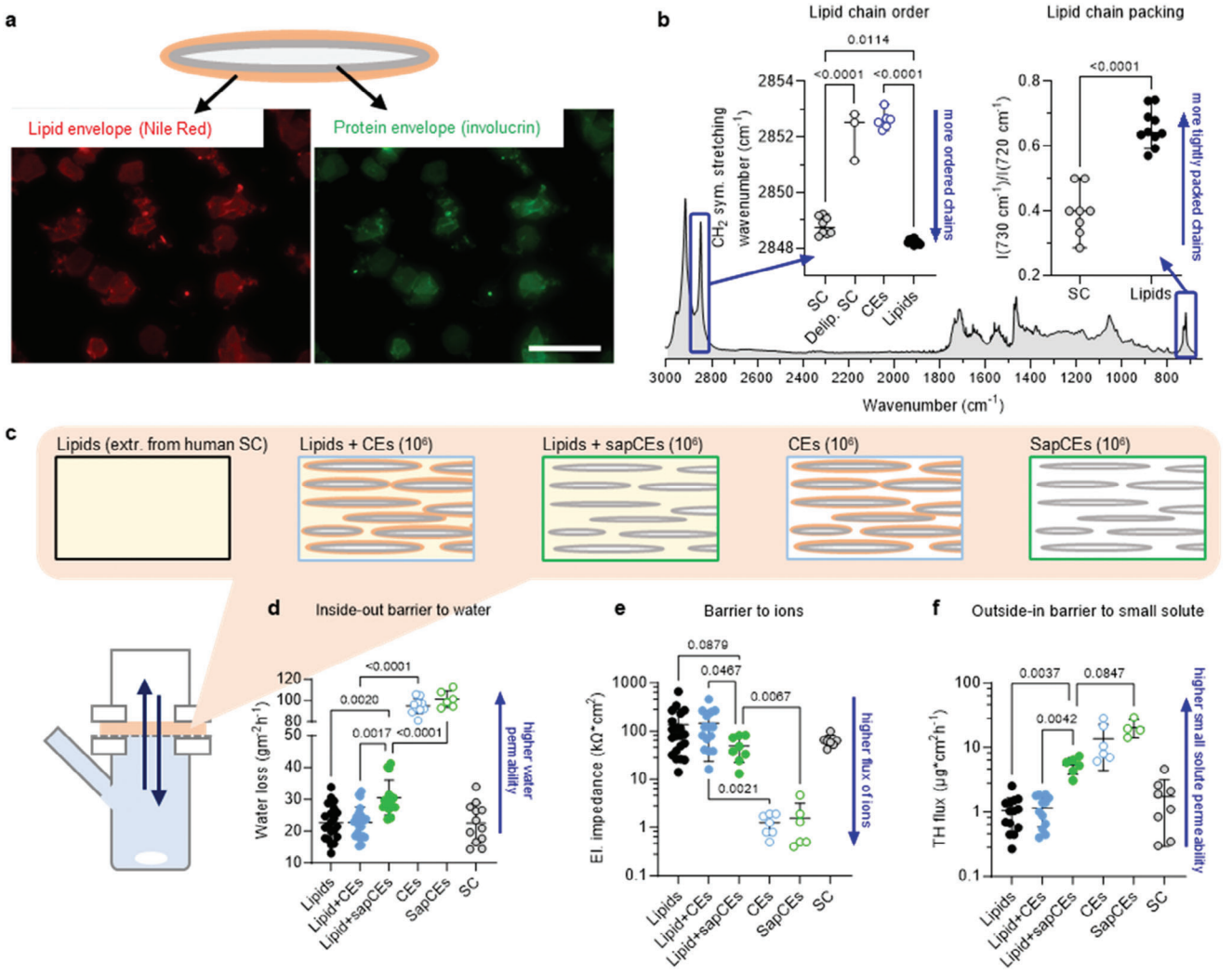

Figure 2. CEs have remarkably fluid lipid chains compared to free SC lipids and alter the lipid lamellae without compromising their permeability. a) The isolated CEs stain for both involucrin and lipids (bar = 50 µm). (b) The SC lipid barrier is a composite of well-ordered and tightly packed extractable lipids and disordered CLE chains on the CE surface. (c) Cartoon of the lipid/CE films and their d) barrier to water loss, e) electrical impedance, f) permeability to TH, a model small solute. Mean ± SD, n is given in each panel as individual points, and *p* values are shown for relevant comparisons (ANOVA).

2.2. CEs with Intact CLE Alter the Lipid Lamellae without Compromising their Permeability

As a proof of concept, we showed that the major SC lipids change their lamellar architecture in the proximity of surface-bound but dynamic lipid-like tails (reverse-phase C18 silica gel) and remain unaffected by a polar surface (normal-phase silica gel; Figure S3, Supporting Information). We then embedded ≈10^6 CEs or sapCEs in 250 µg of isolated and chromatographically purified human SC lipids (a ratio similar to that in the SC). After preliminary studies, we chose to spray lipid solutions together with dispersed CEs versus a sandwich method (using alternate layering of lipids from organic solvents and CEs from aqueous dispersions). Despite this solvent treatment, the CEs remained intact (Figure S2f,g, Supporting Information), confirming their resistance. The lipid films were annealed using an optimized protocol,[23] sandwiched in Franz diffusion cells, and examined for permeability (Figure 2c–f). Water loss values across CEs or sapCEs without free lipids were at their maxima, similar to solvent-extracted or saponified SC. No differences in barrier function were found between lipid films with and without CEs for all three permeability markers (water loss, electrical impedance, and permeability to a model compound theophylline, TH). However, all markers indicated impaired permeability of the lipid films with sapCEs compared to films with CEs with intact CLE. Although direct comparison with in vivo data is not possible, these results are qualitatively consistent with increased skin permeability in diseases with impaired CLE.[27,32]

The properties of the lipid films were investigated by infrared spectroscopy and X-ray diffraction (XRD). The isolated free human SC lipids were well-ordered (**Figure 3**a) with a predominantly orthorhombic packing (Figure 3b) and assembled into LPP with a repeat distance of 13.5 nm (Figure 3c,d), consistent with the literature.[23] The presence of CEs with intact CLE at ≈10^6/250 µg lipids did not alter the conformation or packing of the lipid chains, but the XRD reflections were asymmetric

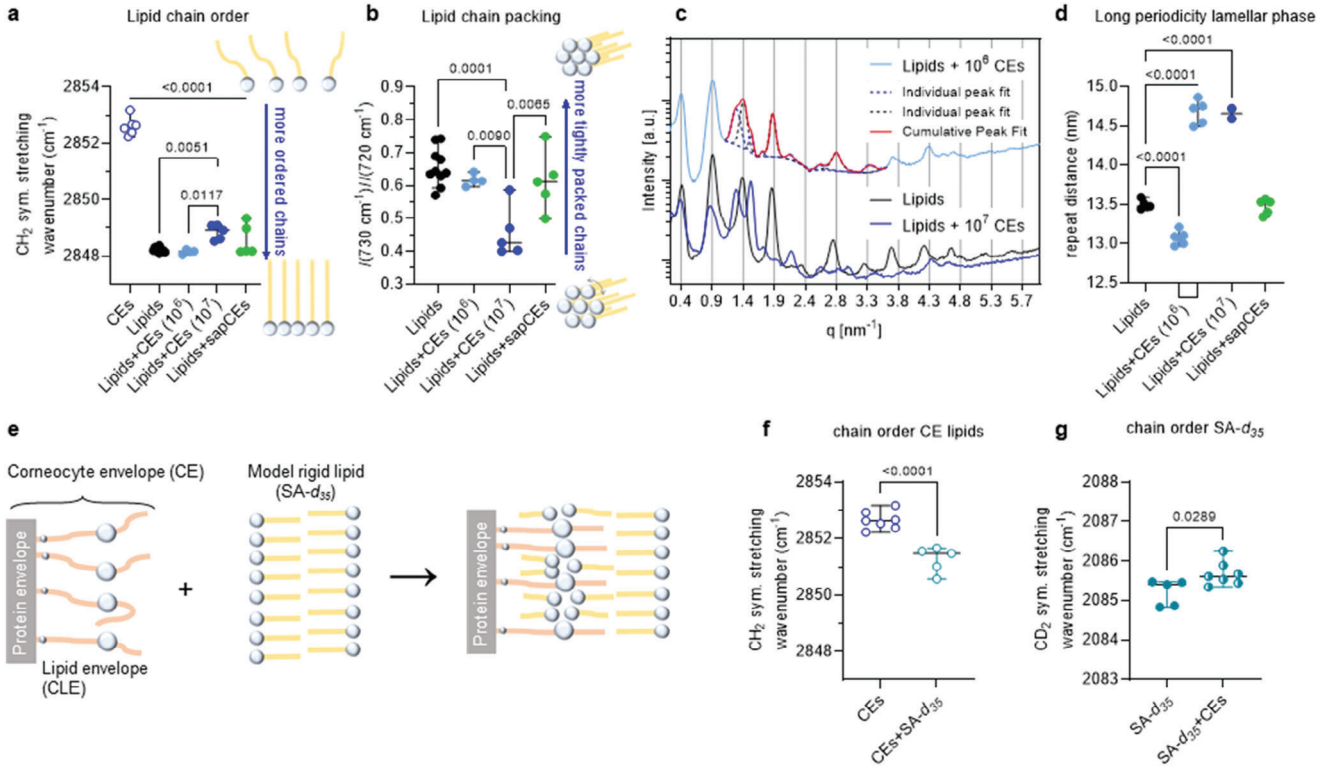

Figure 3. CLEs fluidize and rearrange adjacent free lipids. a) Lipid chain order indicated by the infrared methylene symmetric stretching wavenumbers. b) Relative proportion of a dense orthorhombic chain packing deduced from the relative intensities of the infrared methylene rocking doublet components. c) X-ray diffraction (XRD) patterns showing the lamellar lipid arrangement. d) Repeat distances calculated from the XRD patterns. e) Cartoon of the interaction of CEs with deuterated stearic acid (SA-d_{35}). f) Chain order of CLE lipids and g) SA-d_{35} chains in CEs with/without SA-d_{35}. Mean ± SD, n is given in each panel as individual points, and *p* values are shown for relevant comparisons (a–d, ANOVA, f–g, t-test).

indicating two coexisting phases. Deconvolution of the peaks revealed one phase with a significantly shorter (13.1 nm) and one with a significantly longer repeat distance (14.7 nm) than LPP in lipids without CEs. The sapCEs had no significant effect on the lamellar or lateral arrangement of the free lipids (Figure 3a–d). Thus, CEs with intact CLE induce changes in the lipid lamellar organization while maintaining their low permeability. When the CLE is removed, the sapCEs compromise the lipid barrier despite their somewhat hydrophobic surface.

2.3. CLEs Fluidize and Rearrange Neighboring Free Lipids

To investigate the interactions between CEs and free lipids in their immediate vicinity without the confounding effects of more distant free lipid layers, we increased the number of CEs in the sample tenfold to ≈10^7 CEs per 250 µg lipid (Figure 3a–d). After the incorporation of CEs, infrared spectroscopy revealed more mobile lipid chains and a lower proportion of tight orthorhombic lateral packing compared to lipids without CEs. The 14.7 nm lamellar phase dominated the diffractograms with an additional reflection corresponding to d = 4.1 nm which could not be reliably assigned to any phase.

Repeat distances above 14 nm (or an increase in the LPP repeat distance of 1.2 nm) suggest CLE-induced reorganization/sorting of free lipids. A similar increase in LPP repeat distance was previously reported for SC lipid samples enriched in *ω-O*-acylceramides, where the LPP repeat distance increased by 2.2 nm (from 12.2 nm with 10–30% *ω-O*-acylceramides of the ceramide fraction to 14.4 nm with 90% *ω-O*-acylceramides).[34] A possible mechanism for this increase in repeat distance is the partial stretching of the distal parts of the *N*-acyl chain in *ω-O*-acylceramides (which are largely isotropic at 30% *ω-O*-acylceramides[22]) at their higher concentration or a more pronounced reorganization of these lamellae. A plausible hypothesis is that CLE may attract some free lipids (other than *ω-O*-acylceramides) that can fill the voids between the sparsely covalently bound lipids to form a mature CLE, following a principle similar to the formation of tethered lipid membranes.[35,36] Filling the voids could straighten the ultralong (≈4 nm) CLE chains. This assumption is consistent with the ultrastructural data on CLE maturation in mice from ≈2.3 nm thick immature CLE in the initial SC layers to a 4.4 nm thick mature CLE in healthy mice.[37] The ability of tethered lipids to attract selected lipids, reorganize lipid domains in giant unilamellar vesicles, and, in some cases, completely sequester lipid phases on the interacting surface[38] appears to be highly relevant to the abovementioned CLE behavior. Cytochemical reaction with filipin indicates that CLEs are devoid of cholesterol.[39] Thus free fatty acids or ceramides may be suitable candidates for translocation from free SC lipids into the CLE leaflet, which is supported by their ability to become

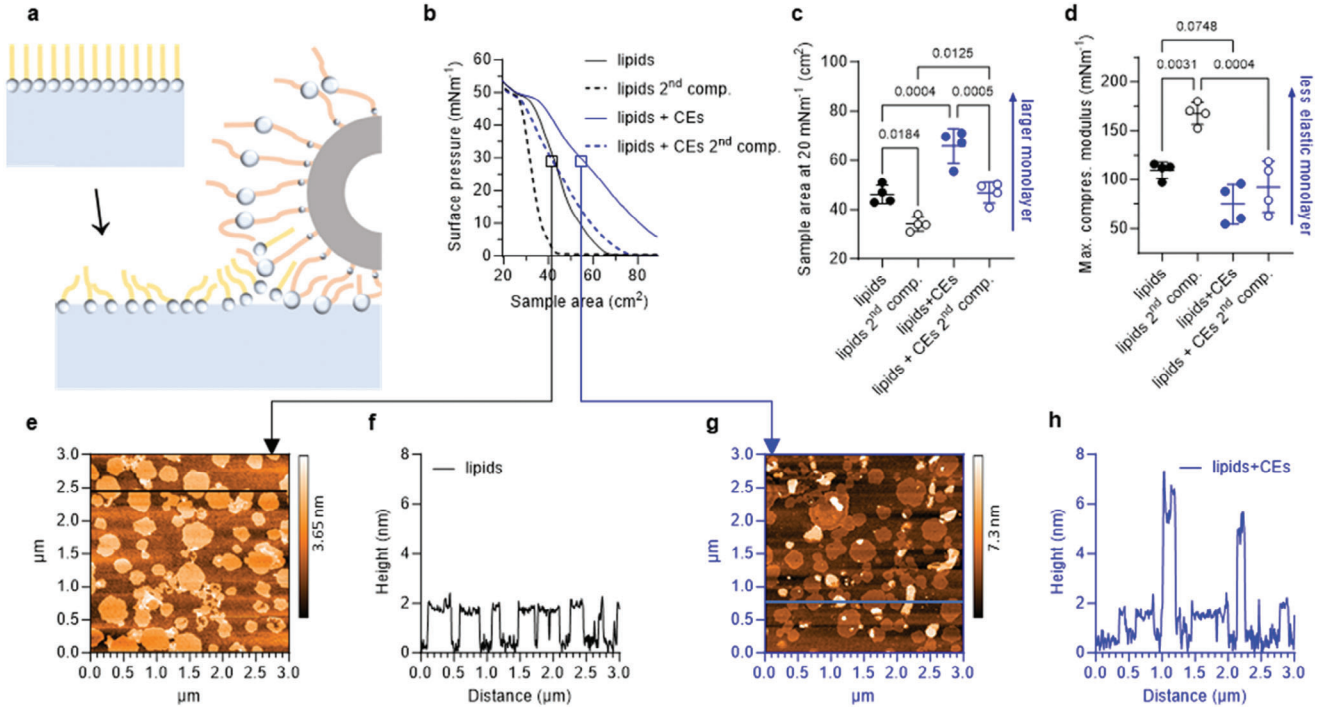

Figure 4. CLEs fluidize lipid monolayers and induce their transformation into multilayers. a) Cartoon illustrating the interaction of SC lipid monolayer with CEs at the air/buffer interface. b) Surface pressure-area isotherms, c) sample areas, and d) compressibility moduli of SC lipids with/without CEs. Mean ± SD, n is given in each panel as individual points, and *p* values are shown for relevant comparisons (ANOVA). e) Representative atomic force micrographs of lipid samples without CEs; the black line indicates the analyzed height profile shown in (f). g) Representative atomic force micrographs of lipid samples with CEs; the blue line indicates the analyzed height profile shown in (h). All AFM samples were prepared at 22 °C and 30 mN m^{-1} and each sample was scanned at least five times.

enriched in the stalk during the first steps of membrane fusion.[40] Interestingly, the filling of the voids between CLE lipids with fatty acids was tentatively proposed two decades ago.[41]

Therefore, for the next experiment, we selected stearic acid, also because of its availability in perdeuterated form. To distinguish the behavior of the CE lipids from the free lipids, we mixed CEs with perdeuterated stearic acid as a model solid lipid at ≈10^7 CEs per 250 μg acid (Figure 3e–g). This interaction indeed resulted in an ordering of the CLE lipids (the CH_2 symmetric stretching wavenumber decreased by 1 cm^{-1} but remained above 2850 cm^{-1}) and a slight disordering of the deuterated stearic acid chains.

Apart from lipid sorting, another possible explanation for the fluidization of the lipid layer adjacent to the CEs is the wetting of the CEs by extracellular lipids. Such protein wetting can change the chain order of the boundary lipids relative to the bulk lipids.[42–44] The adhesion of extracellular lipids to the corneocyte surface will logically be higher when the protein is hydrophobized by covalent CLE lipids than in the absence of CLE. The covalently bound ultralong lipids in CLE may also help to organize domains with different properties (which are likely to be layered rather than laterally segregated in these multilamellar systems[22]) due to the different properties of the ultralong acyl and sphingoid chains, i.e., they may act similarly to surfactants (or lineactants in 2D systems).[45,46]

2.4. The SC Lipid Monolayers with CEs Remain Fluid when Compressed and Rearrange into Multilayers

The CLE-induced lipid fluidization was confirmed using Langmuir monolayers at the air–buffer interface (**Figure** 4a–d). CEs (6×10^5 CEs per 15 μg lipid, i.e., the same ratio as above) increased the lipid area by almost 20 cm^2 (≈10 Å^2/lipid at 20 mN m^{-1}) and monolayer elasticity (lower compressional modulus by 35 mN m^{-1}). CEs alone (6×10^5) did not yield considerable surface pressure when spread at ≥20 cm^2. Since our skin is often subjected to mechanical stress, we further investigated the behavior of Langmuir monolayers during repeated compressions. Expansion of the compressed film and repeated compression showed that without CEs, some of the lipid chains rearrange or are squeezed out during the first compression (by 25% smaller area per lipid), rendering the resulting lipid film more rigid (the increase in compressional modulus from 109 to 168 mN m^{-1}). This behavior resembles the behavior of lung surfactant lipids, which led to the early squeeze-out hypothesis.[47] Analysis of a carefully sampled subphase beneath a monolayer at 40–45 mN m^{-1} showed that only 3.7% of the total lipid was lost to the subphase during compression. The 25% reduction in monolayer area can therefore be explained by monolayer buckling, folding, and formation of multilayer lipid structures attached to the monolayer at high surface pressures.[48] Unlike phospholipids, these multilayers do not fully respread on expansion, which may be due to the ceramides forming extended conformations[19,49–52]

that can effectively zipper and stabilize the folded multilayers. CEs prevented the formation of incompressible condensed lipid phases, even at high surface pressures, as evidenced by the maximum compression modulus values below 100 mN m^{-1}, despite a similar reduction in area. These results suggest that the lipid layer facing the corneocyte remains fluid during compression, which may reasonably explain the ability of the SC to adapt to mechanical stresses induced by skin folding and stretching during physiological activities. Thus, the attenuated CLE may contribute to skin fragility in patients with ichthyoses who have mutations in lipid pathways converging on the CLE.[25]

In previous studies, we described the ability of monolayers of isolated human SC lipids transferred to a solid substrate to remodel into multilayers. This spontaneous transformation was never observed at laboratory temperature, but only at higher temperatures when a significant fraction of the lipids lost their tight orthorhombic arrangement.[49,53] Since the above results suggest less tight ordering and higher mobility of lipid chains in the presence of CEs, we hypothesized that remodeling into multilayers could occur even at laboratory temperature in the presence of CEs.

We therefore transferred monolayers from the buffer–air interface at 30 mN m^{-1} onto freshly cleaved mica using the Langmuir–Blodgett technique and scanned them with AFM (Figure 4e–h). The SC lipid monolayer at 22 °C contained two domains (Figure 4e,f), with the lighter domains (of the order of tens to hundreds of nm in diameter) ≈2 nm (1.6–2.2 nm) higher than the darker regions. The lower domains are likely to be rich in cholesterol, fatty acids, and ceramides with shorter acyls, and the higher domains are rich in lipids with very long acyls. Occasional bright spots protruding ≈1.5–2 nm above the surface may correspond to ultralong ω-O-acylceramides. The lipid monolayer sample with CEs contained large objects corresponding to CEs with a rough surface on which we could not observe fine details in the lipid arrangement. However, when we scanned the regions between the CEs, we consistently found multilayered islands in the monolayer background (the lightest formations in Figure 4g protruding 6–9 nm above the surrounding monolayer, Figure 4h) The monolayer background had two domains very similar to those of lipids without CEs, only the difference in their heights was slightly smaller with CEs, ≈0.9–1.7 nm. The driving force for the reorganization is likely to be the propensity of ceramide to form a splayed-chain (extended) conformation with its asymmetric chains pointing in opposite directions in order to relieve the stress resulting from its unfavorable packing ratio (smaller cross-section of the polar head compared to the two chains). This extended conformation has been experimentally observed[19,49,50] and proposed to explain the electron microscopic patterns in the SC extracellular matrix.[51,52]

This spontaneous transformation of the SC lipid monolayer into a multilayer, which only occurs in the presence of CEs at a given temperature, is a further indication that CEs alter the mechanical properties of lipids. These results are consistent with the observation of similar transformations in Langmuir–Blodgett films of fatty acid salts, where films deposited from the hexagonal phase spontaneously transform into multilayers, whereas films deposited from the (pseudo)orthorhombic phase, where the tight arrangement of lipids prevents rotational motions and greatly increases viscosity, remain stable.[54] The observed monolayer transformation suggests that the lipid layer facing the corneocyte is a highly dynamic environment that remains fluid during compression. In addition, such fluid lipids surrounding the corneocyte are consistent with the SC enzyme activity, which would otherwise decrease rapidly in densely packed lipids.[55]

2.5. Unbound CLE Lipids Do Not Reproduce CLE-Mediated Effects

Finally, we investigated whether the observed lipid fluidization was indeed mediated by lipids covalently bound in CLE or whether it could be reproduced by the unbound CLE components. The unbound CLE was approximated by a mixture of ω-hydroxy ceramides (with 32-hydroxydotriacontanoyl chains), ω-hydroxy fatty acid (32-hydroxydotriacontanoic acid), and free fatty acids in an 88:7:5 molar ratio[56] and mixed with isolated human SC lipids in a 1:20 molar ratio. The addition of unbound CLE lipids did not alter the permeability of the free lipids to any of the three markers used above (Figure S4, Supporting Information). In contrast to CEs, the unbound CLE lipids neither fluidized the free lipids, changed the proportion of dense orthorhombic packing, nor changed the long periodicity phase repeat distance. Thus, in agreement with the disrupted skin lipid barrier in patients with ichthyosis,[25,27] the individual unbound chemical structures of the CLE are not sufficient for the CLE-mediated fluidization/unjamming of the free lipid aggregates; the CLE must be immobilized on the corneocyte surface.

2.6. Maturation of the Lipid Barrier

This described fluidized or unjammed state of the SC extracellular matrix is obviously transient during its remodeling in the lower layers of the SC, as the mature lipid skin barrier is characterized by a predominance of very tightly arranged lipid chains in orthorhombic packing and low permeability. The nanomechanical properties of corneocytes, including CEs, also change (the tissue becomes stiffer) as the cells mature and move closer to the body surface.[57] This process, which can be described as jamming, i.e., the effective freezing of a tissue into a preferred arrangement, typically follows a transient unjamming during tissue development.[12] The logical question, however, is what enables this jamming process in the SC extracellular matrix. Jančálková et al recently highlighted the importance of the hexagonal to orthorhombic packing transition of SC lipids,[53] which occurs at ≈35 °C and is significantly modulated by hydration. With decreasing temperature or hydration, which physiologically occurs towards the skin surface, the dynamics of the lipid chains decrease and the activation energy for the transport of a subset of substances also increases, in line with the concept of jamming and the functional role of the skin barrier.

Thus, it appears that the composition of the extracellular lipids of the SC has been specifically tuned not only to functionally protect the human body from a desiccating environment but also to ensure their certain malleability during barrier assembly and subsequent effective solidification response to subtle changes in temperature and hydration upon movement closer to the skin surface.[53] Notably, this solidification is most likely

confined to the acyl chain-rich leaflets of the multilayered architecture of this extracellular lipid matrix, whereas the sphingoid base-rich leaflets and the linoleate-rich slab are still dynamic environments.[19,22] The physiological role of this isotropic linoleate slab between very rigid acyl chains, which closely resembles (and is formed from) a lipid droplet, is not yet known. It is possible that the isotropic slab may reduce interlayer friction, which can otherwise be quite high due to the interdigitation of different acyl lengths. Such low friction is probably already necessary for the budding of lipid precursor lamellae into lamellar bodies, during the remodeling of lipid lamellae into a barrier (because interlayer friction would slow down lipid redistribution after local membrane modification presumably induced by CLE[58]), and probably also contributes to the overall mechanical properties of extracellular lipids that might otherwise be too brittle.

3. Conclusion

As proposed a century ago[59] and more recently,[13,15] the shaping of living tissues shares fundamental physical principles with the sculpting of many inert materials, where molding them into functional shapes requires the constituent material to locally flow like a fluid while maintaining overall mechanical integrity like a solid. During the formation of a competent skin barrier, massive remodeling of the extracellular matrix occurs,[11] which appears to be consistent with the current concept of unjamming transition in biology.[12] Although this concept has been described for cellular collectives, we propose here that it can be well applied to extracellular matrix components. In previous work, we have shown that these lipids, whose rigidity is well beyond that of classical cell membranes, require transient partial fluidization to become malleable that is to arrange themselves without permeability defects.[23] In that work we modeled fluidization by elevated temperature; here we propose that the covalent lipid coat on the corneocyte surface, CLE, may physiologically contribute to this process.

We show here that CLE is not a rigid scaffold but a sparse template that can fluidize and rearrange the proximal free extracellular lipids. The observed characteristics of SC lipids in the presence of CEs, such as decreased lipid chain order, increased chain rotations due to the transition of part of the chains from orthorhombic to hexagonal lateral packing, increased monolayer elasticity as well as the ability to spontaneously transform from monolayer to multilayer, clearly indicate a change in the mechanical properties of these lipids[60] in terms of increased malleability to organize the free lipids into a functional protective barrier without significant defects. This tethered lipid layer may also accommodate the peptide and protein structures more readily than the rigid extracellular lipids and adapt to mechanical stress caused by hydration-induced changes in corneocyte shape and physiological skin stretching.

It is also interesting to note the similarities in the barriers to the terrestrial environment that have evolved in very different species, including plants and arthropods.[61,62] All these barriers to the transport of substances, especially to water loss, are based on extracellular lipids with long to very long aliphatic chains from the group of nonpolar or polar non-swelling lipids. These lipids, like human SC lipids, are arranged in lamellae parallel to the underlying surface, and in plants, for example, we find an orthorhombic arrangement of aliphatic chains. The adhesion of these lipid lamellae to the integument is somehow secured (e.g., by the cutin network in plants) and the polymeric substrate together with the lipids thus forms a composite material, not unlike the protein–lipid complex of the human skin barrier. The mechanisms of lipid transport and arrangement in these waterproofing barriers are not yet fully understood, and it is possible that the concept of unjamming followed by jamming may be a universal principle of water barrier formation in many organisms.

In conclusion, our in vitro results suggest for the first time the existence of an unjamming transition in skin barrier development, provide a new testable hypothesis regarding the role of CLE in the skin barrier, and inspire the design of new functional materials.

4. Experimental Section

Material: Ceramide standards for analysis were purchased from Avanti Polar lipids (Alabaster, AL, USA) or synthesized in-house by an *N*-acylation of sphingoid bases with appropriate fatty acids using *N*-(3-dimethylaminopropyl)-*N*′-ethylcarbodiimide and 1-hydroxybenzotriazole hydrate. ω-Esterificated and ω-hydroxylated ceramides were prepared according to a modified procedure based on Opálka et al.[63] Other chemicals and solvents (analytical or HPLC grade) were purchased from Merck (Schnelldorf, Germany), and inorganic salts for the preparation of buffers were obtained from Lachema (Neratovice, Czech Republic). Mouse monoclonal anti-involucrin antibody [SY5] and Alexa Fluor 488-labeled secondary antibody (goat polyclonal secondary antibody to mouse IgG) were purchased from Abcam, Cambridge, UK. Water was purified through a Millipore Q purification system.

Isolation of Human SC and SC Lipids: Human skin was obtained from patients who underwent abdominal plastic surgery and provided their written informed consent. The procedure was approved by the Ethics Committee of the Sanus First Private Surgical Centre, Czech Republic (No. 5/4/2018), and performed according to the principles of the Declaration of Helsinki. The skin was separated from the subcutaneous fat with a scalpel within 6 h of the surgery and gently wiped with an acetone-soaked paper towel to remove residual fat. The epidermis was separated from the dermis using 2.4 mg mL^{-1} dispase II with 50 mg L^{-1} gentamicin solution overnight. The epidermis was incubated in 0.5% trypsin solution with gentamicin in PBS at 32 °C overnight to isolate the SC, and the remaining keratinocytes were removed from the SC sheets with cotton buds. Lipids were extracted from the SC samples pooled from six donors using chloroform//methanol mixtures (2:1, 1:1, and 1:2 v/v)[64] and purified by column chromatography. The correct composition and purity of the isolated lipids were confirmed by high-performance thin-layer chromatography using authentic standards[65] and LC-MS^2, see below. For pilot experiments, the ceramide fraction was isolated.[66]

Liquid Chromatography Coupled to Tandem Mass Spectrometry (LC-MS^2) Analysis of Ceramides: Isolated human SC lipids (10 µg at 1 mg mL^{-1} in $CHCl_3$ were mixed with 100 µL of the internal standard mixture (ceramides NS (d18:1/14:0), NS (d18:1/19:0), NS (d18:1/25:0), NS (d18:1/31:0), NdS (d18:0/14:0), NP (t18:0/14:0), EOS (d18:1/h29:0/18:2) at 200 nmol L^{-1}) and the solvents were evaporated under a gentle nitrogen stream. The sample was reconstituted in 500 µL $CHCl_3$/MeOH 1:9 (v/v) and analyzed on Shimadzu Prominence HPLC with LCMS 8050 instrument (Shimadzu, Kyoto, Japan). Ceramides were separated on an Ascentis C18 column (15 cm × 2.1 mm; 3 µm, Supelco, USA) using a gradient between 57% solvent A (50% MeOH, 50% water) and 99% solvent B (99% isopropanol, 1% MeOH), both containing 10 mM ammonium formate and 0.1% formic acid as additives, at a flow rate of 0.2 mL min^{-1} at 30 °C. Table S1 (Supporting Information) shows the lipids analyzed, their corresponding transitions (using multi-reaction

monitoring), and retention times. Quantification was performed using the above internal standards and the following external standards: Ceramide NS(d18:1;24:0), NdS(d18:0;24:0), NP(t18:0;24:0), NH(t18:1;24:0), EOS(d18:1;h32:0;18:2), EOP(t18:1;h32:0;18:2), EOdS(d18:0;h32:0;18:2), OS(d18:1;h32:0), OdS(d18:0;h32:0), OP(t18:0;h32:0), AS(d18:1;h24:0), AdS(d18:0;h24:0), AP(t18:0;h24:0). Correction for increasing sphingolipid chain length was used for quantification.

Isolation of Corneocyte Envelopes (CEs): To isolate CEs without traces of surfactants, the published methods were tested and then modified.[67,68] To avoid SDS, delipidated SC sheets were dispersed in the extraction buffer consisting of 20 mM Tris HCl, 5 mM ethylenediaminetetraacetic acid, 10 mM DL-dithiothreitol, and 8 mM DDAO at pH 7.4 stirred at 45–50 °C for 2–3 days and filtered using nylon net filters with 41 µm pore size (Fisher Scientific EU). The filtrate was centrifuged at 14 000 rpm for 20 min to pellet the CEs. These pellets were washed three times with a washing buffer (20 mM Tris HCl, 5 mM ethylenediaminetetraacetic acid, and 10 mM DL-dithiothreitol at pH 7.4) and the CEs were stored in the washing buffer at 4 °C. For counting with a hemocytometer (Merck, Schnelldorf, Germany), the CEs were centrifuged and the pellet was resuspended in PBS.

To isolate saponified CEs (sapCEs, with the CLE removed), extracted SC sheets were suspended in 1 M NaOH in methanol (1:9, v/v) at 45 °C for 1 h to saponify the ester bonds and remove the covalently bound lipids from the corneocytes. The mixtures were acidified to pH 4 with 2 M HCl,[56] filtered through nylon net filters with 41 µm pore size (Fisher Scientific EU), and washed thoroughly with deionized water. The saponified SC samples were then stirred in the extraction buffer at 45–50 °C for 48 h, filtered, and centrifuged at 14 000 rpm for 10 min to collect the sapCEs. The sapCEs were washed and counted as described above.

Isolated (sap)CEs on a glass slide were stained with 20 µL of an anti-involucrin antibody [SY5] at 4 °C overnight, followed by Alexa Fluor 488 labeled secondary antibody at room temperature.[69,70] After 1 h, (sap)CEs were washed with water, stained with Nile Red (75% glycerol with 20 µL mL^{-1} of a stock solution of 500 µg mL^{-1} Nile Red in acetone) for 10 min, and washed again with water to remove excess staining. The samples were observed with a Nikon Ti-E fluorescence microscope (Nikon, Japan) equipped with CoolLED pE-300 fluorescence source (CoolLED, United Kingdom) and cooled sCMOS camera Andor Zyla 5.5 (Oxford Instruments, United Kingdom) using FITC and Cy3 filter cubes. Photomicrographs were taken with a Nikon Plan Apo λ 20×/0.75 or Nikon Plan Apo λ 40×/0.95 dry lenses. Microscope control and image processing were performed using NIS Elements AR 4.2 (Laboratory Imaging, Czech Republic).

Lipid Models: First, to investigate the interaction of SC lipids with surface-anchored alkyl chains, normal phase and C_{18} reverse phase silica gel particles (5–7 µm diameter; either 0.16 or 0.5 mg) were first embedded in lipid films (1.35 mg cm^{-2}) composed of isolated human SC ceramide fraction,[66] free fatty acid mixture,[71] and cholesterol in a 1:1:1 molar ratio with 5 wt.% of cholesteryl sulfate sodium salt.

For lipid models with CEs or sapCEs, (sap)CEs were embedded in thin films of isolated human SC lipids. For this proof-of-concept study, the CEs were treated purely as physical objects that may or may not interact with the lipids. Lipids (without CEs) and (sap)CEs without lipids were studied as controls. The (sap)CEs were counted, the desired amounts were centrifuged, the supernatants were discarded, and the pellets were air-dried. Lipids were dissolved in 2:1 hexane:ethanol (v/v) at 0.83 mg mL^{-1}. The dried (sap)CEs were mixed with the lipid solution (10^6 or 10^7 per 250 µg of lipids) or with the solvent alone.

For models with unbound CLE lipids, unbound CLE was approximated by a mixture of ceramides/32-hydroxydotriacontanoic acid/free fatty acids at a 88:7:5 molar ratio[56] and mixed with isolated human SC lipids at a 1:20 molar ratio in 2:1 hexane:ethanol (v/v). The ceramide mixture contained 32-hydroxydotriacontanoyl-(*2S,3R,E*)-sphingosine, 32-hydroxydotriacontanoyl-(*2S,3S,4R*)-phytosphingosine and 32-hydroxydotriacontanoyl-(*2S,3R*)-dihydrosphingosine in an 89:7.8:3.2 molar ratio. The synthesis of these lipids will be reported elsewhere. The free fatty acid mixture contained myristic, palmitic, stearic, oleic, icosanoic, and docosanoic acid in an 8.3:35.5:20.9:17:14.2:4.1 molar ratio.

The samples were sprayed in three portions (250 µg lipids for the CE samples, or 1.35 mg lipids for the unbound CLE or silica gel samples) onto 1 cm^2 of Esco 22 × 22 mm^2 microscope coverslips (Erie Scientific LLC, Portsmouth, New Hampshire, USA—for infrared spectroscopy or XRD) or Nuclepore track-etched polycarbonate membranes with a 0.015 µm pore size (Whatman, Kent, Maidstone, United Kingdom—for permeation experiments) at a sample flow rate of 10.2 µL min^{-1} using nitrogen as a carrier gas with Linomat 5 (Camag, Muttenz, Switzerland). Samples were vacuum-dried with P_4O_{10} and solid paraffin and stored at 4 °C. Before use, the samples were annealed at 70 °C for 10 min and slowly cooled to 32 °C.

X-ray Diffraction (XRD): Samples for X-ray diffraction measurements were sealed in 1.5 mm diameter quartz (Capillary Tube Supplies Ltd, Bodmin, UK) or borosilicate capillaries (WJM-Glas/Müller GmbH, Berlin, Germany) and the data were collected at ambient temperature and humidity using a Bruker Nanostar small-angle X-ray scattering instrument (Bruker Corporation, Billerica, MA, USA). The instrument was equipped with a microfocus source (λ = 0.15418 nm; Incoatec High Brilliance) and a 2D position-sensitive detector (Vantec 2000, Bruker AXS). Spatial correction and flood file correction were used to correct the 2D scattering image. The detector was calibrated using silver behenate (Alfa aesar GmbH&Co, Karlsruhe, Germany). Collected X-ray scattering data were radially integrated using Fit2D software (Andy Hammersley, European Synchrotron Radiation Facility, Grenoble, France).

The X-ray data in Figure S2 (Supporting Information) were collected at ambient temperature and humidity with an X'Pert PRO θ–θ diffractometer (PANalytical B.V., Almelo, The Netherlands) with parafocusing Bragg–Brentano geometry using CoKα radiation (λ = 0.17 903 nm, U = 40 kV, I = 30 mA). The samples were measured in modified sample holders in the angular range of 0.6°–30° (2θ). The samples were scanned with an ultrafast position-sensitive linear (1D) PIXCEL detector with a step size of 0.026° (2θ) and a counting time of 0.155 s/step. Data were analyzed using X'Pert Data Viewer software (PANalytical B.V., Almelo, Netherlands).

The X-ray diffraction curves shown are the raw scattered intensity without normalization as a function of the magnitude of the scattering vector q (nm^{-1}), which is proportional to the scattering angle 2θ according to the equation: $q = 4\pi \sin\theta/\lambda$ (λ is the wavelength of the X-ray). The repeat distance d (nm) characterizes the regular spacing between adjacent scattering planes arranged in a 1D lattice. The scattering patterns of the lamellar structure show a series of Bragg reflections with reciprocal spacings in characteristic ratios of $q_n = 2\pi n/d$ (diffraction index n = 1, 2, 3...). The repeat distance d was obtained from the slope a of a linear regression function of the dependence $q_n = an + q_0$, where q_0 is a constant corresponding to a shift of the origin, according to the equation $d = 2\pi/a$.

Fourier Transform Infrared Spectroscopy: Infrared spectra were collected with a Nicolet 6700 spectrometer (Thermo Scientific, USA) equipped with a single-reflection MIRacle ATR ZnSe crystal (PIKE Technologies, Madison, USA). A constant pressure clamping mechanism was used. Spectra were generated from 256 scans collected at a 2 cm^{-1} resolution in the range of 4000 to 600 cm^{-1} at ambient temperature and analyzed using Bruker OPUS software.

Water Loss, Electrical Impedance, and Permeability of Lipid Films: Lipid films with or without (sap)CEs (≈10^6 per 250 µg of lipid) on Nuclepore filters were placed in Teflon holders with a 0.5 cm^2 circular opening. (sap)CEs without lipids (≈10^6 per sample) were used as negative controls. The holders were mounted in the Franz diffusion cells, with the samples facing the donor compartment. The acceptor compartment was filled with PBS at pH 7.4 (≈6.5 mL, measured individually for each cell) and stirred at 32 °C. The reason for this pH below the bulk lipid film was to simulate the near-neutral environment in the viable epidermis (i.e., below the stratum corneum) during the permeation experiment. An additional experiment comparing the permeability of the lipid films with and without CEs with an acceptor phase at either pH 7.4 or 5.5 was also performed. Some insignificant trends towards overall lower permeability at acidic pH were noted but without any difference between the lipid and lipid+CEs groups (data not shown). After an overnight equilibration, water loss and electrical impedance were measured. First, the donor compartment of the Franz cells was removed, and water loss was measured with an AquaFlux AF 200 instrument (Biox Systems Ltd, UK) using the condenser-chamber

measurement method at 30–36% relative air humidity and 24–26 °C.[72] Next, 0.5 mL PBS was added to the donor compartment and, after 1 h of equilibration, electrical impedance was measured using an LCR meter 4080 (Conrad Electronic, Hirschau, Germany) with each electrode inserted in the donor and acceptor phases. Next, 100 µL of 5% theophylline (TH) in PBS was applied to the lipid films. For the unbound CLE experiments, TH was applied in 60% aqueous propylene glycol. Acceptor phase samples (300 µL) were collected at 2, 4, 6, and 8 h and replaced with the same amount of fresh PBS. TH was quantified by HPLC,[73] corrected for acceptor sample replacement, and plotted against time. The TH flux values were calculated as the slopes of the linear parts of the permeation profiles.

Langmuir Monolayers: Langmuir–Blodgett trough (KSV NIMA, Espoo Finland) was used to investigate the interfacial lipid behavior. Lipids (15 µL of a 1 mg mL^{-1} solution in chloroform/methanol 2:1 v/v) with or without CEs (6×10^5) were carefully spread on the acetate buffer saline (pH 5.5) subphase at 22 °C and the solvents were allowed to evaporate for 20 min. The samples were compressed (first compression) and then barriers were expanded followed by second compression at 20 mm min^{-1}, the surface pressure (π) was measured using a Pt Wilhelmy plate and was plotted against the trough area.

Atomic Force Microscopy (AFM): For AFM measurements, the lipid monolayers were compressed to 30 mN m^{-1} surface pressure and after 15 min were deposited by Langmuir–Blodgett techniques onto freshly cleaved mica support (15×15 mm^2, SPI Supplies, West Chester, PA USA) by lifting the mica from the subphase through the lipid monolayer at a speed of 1 mm min^{-1} and constant surface pressure. Samples were allowed to dry for 20 min, further dried under a stream of nitrogen, and stored in the dark at laboratory temperature under an argon atmosphere prior to measurement. The prepared samples were visualized by atomic force microscopy (AFM) using the Nanosurf easyScan 2 FlexAFM device (Nanosurf AG, Switzerland). Scans were performed in static force mode (contact mode) using the ContAl-G probe (Budget Sensors, Bulgaria) with a nominal spring constant of 0.2 N m^{-1} and a resonant frequency of 13 kHz at a resolution of 512×512 points.

Statistical Analysis: Two groups were compared using an unpaired two-tailed t-test; three or more groups using ANOVA with Tukey´s multiple comparison test; $p < 0.05$ was considered statistically significant (GraphPad Prism v.9 or 10, GraphPad Software, USA). The data are presented as the means ± standard deviation (SD); the number of replicates (n) is specified in each Figure.

Supporting Information

Supporting Information is available from the Wiley Online Library or from the author.

Acknowledgements

This work was supported by the Czech Science Foundation (22-20839K), Charles University (SVV 260661), the project EFSA-CDN (CZ.02.1.01/0.0/0.0/16_019/0000841), and InoMed (No. CZ.02.1.01/0.0/0.0/18_069/0010046) co-funded by the European Union. The authors thank Iva Vencovská, Lucia Dulanská, Niloofar Asgari, Inés Manchón Mariño, Frederika Tkáčová, Táňa Ryantová, Monika Kopečná, Iva Hrdinová, Paula Hyks, and Daniel Gitschthaler for their assistance with infrared spectroscopy, lipid models, HPTLC, deuterated SDS experiment, and X-ray diffraction measurements, Dr. Mila Boncheva for fruitful discussions and Dr. Russell Kitson for language editing.

Open access publishing facilitated by Univerzita Karlova, as part of the Wiley - CzechELib agreement.

Conflict of Interest

The authors declare no conflict of interest.

Author Contributions

A.D., A.M., and P.P. contributed equally to this work. K.V. conceived and designed this project. A.D., A.M., and A.P. developed and validated methods for CE isolation and characterization. A.D. and A.M. prepared lipid/CE samples and analyzed permeabilities. P.P., H.P., L.D., and J.M. performed and analyzed X-ray diffraction. A.K. performed infrared spectroscopy. A.D., A.M., and P.J. performed monolayer studies. M.M. performed fluorescence microscopy. L.O. prepared and analyzed samples with non-bound CLE and performed LC-MS/MS analysis. P.S. performed AFM studies. K.V. analyzed infrared data and wrote the manuscript with contributions from all authors.

Data Availability Statement

The data that support the findings of this study are available from the corresponding author upon reasonable request.

Keywords

barrier, lipid assembly, membrane remodeling, permeability, template

Received: September 6, 2023
Revised: December 18, 2023
Published online: January 20, 2024

[1] E. Candi, R. Schmidt, G. Melino, *Nat. Rev. Mol. Cell Biol.* **2005**, *6*, 328.
[2] T. Matsui, M. Amagai, *Int. Immunol.* **2015**, *27*, 269.
[3] P. M. Elias, *Int. J. Dermatol.* **1981**, *20*, 1.
[4] M. Rabionet, K. Gorgas, R. Sandhoff, *Biochim. Biophys. Acta* **2014**, *1841*, 422.
[5] B. Breiden, K. Sandhoff, *Biochim. Biophys. Acta* **2014**, *1841*, 441.
[6] J. van Smeden, M. Janssens, G. S. Gooris, J. A. Bouwstra, *Biochim. Biophys. Acta* **2014**, *1841*, 295.
[7] A. Kovacik, M. Kopecna, K. Vavrova, *Expert Opin. Drug Deliv.* **2020**, *17*, 145.
[8] J. A. Bouwstra, G. S. Gooris, J. A. van der Spek, W. Bras, *J. Invest. Dermatol.* **1991**, *97*, 1005.
[9] J. A. Bouwstra, A. Nadaban, W. Bras, C. McCabe, A. Bunge, G. S. Gooris, *Prog. Lipid Res.* **2023**, *92*, 101252.
[10] P. M. Elias, R. Gruber, D. Crumrine, G. Menon, M. L. Williams, J. S. Wakefield, W. M. Holleran, Y. Uchida, *Biochim. Biophys. Acta* **2014**, *1841*, 314.
[11] A. Narangifard, C. L. Wennberg, L. den Hollander, I. Iwai, H. Han, M. Lundborg, S. Masich, E. Lindahl, B. Daneholt, L. Norlen, *J. Invest. Dermatol.* **2021**, *141*, 1243.
[12] L. Atia, J. J. Fredberg, N. S. Gov, A. F. Pegoraro, *Cells Dev* **2021**, *168*, 203727.
[13] P. F. Lenne, V. Trivedi, *Nat. Commun.* **2022**, *13*, 664.
[14] J. A. Mitchel, A. Das, M. J. O'Sullivan, I. T. Stancil, S. J. DeCamp, S. Koehler, O. H. Ocana, J. P. Butler, J. J. Fredberg, M. A. Nieto, D. Bi, J. A. Park, *Nat. Commun.* **2020**, *11*, 5053.
[15] A. Mongera, P. Rowghanian, H. J. Gustafson, E. Shelton, D. A. Kealhofer, E. K. Carn, F. Serwane, A. A. Lucio, J. Giammona, O. Campas, *Nature* **2018**, *561*, 401.
[16] R. J. Tetley, M. F. Staddon, D. Heller, A. Hoppe, S. Banerjee, Y. Mao, *Nat. Phys.* **2019**, *15*, 1195.
[17] L. Oswald, S. Grosser, D. M. Smith, J. A. Kas, *J. Phys. D. Appl. Phys.* **2017**, *50*, 483001.
[18] J. M. Meyer, K. Vavrova, F. P. W. Radner, H. Schneider, A. Dick, T. M. Mauro, P. M. Elias, *J. Invest. Dermatol.* **2023**, *143*, 332.

[19] O. Engberg, A. Kovacik, P. Pullmannova, M. Juhascik, L. Opalka, D. Huster, K. Vavrova, *Angew. Chem. Int. Ed. Engl.* **2020**, *59*, 17383.
[20] Q. D. Pham, E. H. Mojumdar, G. S. Gooris, J. A. Bouwstra, E. Sparr, D. Topgaard, *Q. Rev. Biophys.* **2018**, *51*, e7.
[21] A. Paz Ramos, G. Gooris, J. Bouwstra, M. Lafleur, *J. Lipid Res.* **2018**, *59*, 137.
[22] F. Fandrei, T. Havrisak, L. Opalka, O. Engberg, A. A. Smith, P. Pullmannova, N. Kucerka, V. Ondrejcekova, B. Deme, L. Novakova, M. Steinhart, K. Vavrova, D. Huster, *J. Lipid Res.* **2023**, *64*, 100356.
[23] I. Sagrafena, G. Paraskevopoulos, P. Pullmannova, L. Opalka, A. Novackova, O. Lourantou, K. Vavrova, *J. Invest. Dermatol.* **2022**, *142*, 2036.
[24] D. C. Swartzendruber, P. W. Wertz, K. C. Madison, D. T. Downing, *J. Invest. Dermatol.* **1987**, *88*, 709.
[25] D. Crumrine, D. Khnykin, P. Krieg, M. Q. Man, A. Celli, T. M. Mauro, J. S. Wakefield, G. Menon, E. Mauldin, J. H. Miner, M. H. Lin, A. R. Brash, E. Sprecher, F. P. W. Radner, K. Choate, D. Roop, Y. Uchida, R. Gruber, M. Schmuth, P. M. Elias, *J. Invest. Dermatol.* **2019**, *139*, 760.
[26] M. Akiyama, *J. Dermatol. Sci.* **2017**, *88*, 3.
[27] M. Pichery, A. Huchenq, R. Sandhoff, S.-M. Freire, S. Zaafouri, L. Opalka, T. Levade, V. Soldan, J. Bertrand-Michel, E. Lhuillier, G. Serre, A. Maruani, J. Mazereeuw-Hautier, N. Jonca, *Hum. Mol. Genet.* **2017**, *26*, 1787.
[28] A. Rath, M. Glibowicka, V. G. Nadeau, G. Chen, C. M. Deber, *Proc. Natl. Acad. Sci. USA* **2009**, *106*, 1760.
[29] M. Janssens, J. van Smeden, G. S. Gooris, W. Bras, G. Portale, P. J. Caspers, R. J. Vreeken, T. Hankemeier, S. Kezic, R. Wolterbeek, A. P. Lavrijsen, J. A. Bouwstra, *J. Lipid Res.* **2012**, *53*, 2755.
[30] M. Jarnik, M. N. Simon, A. C. Steven, *J. Cell Sci.* **1998**, *111*, 1051.
[31] D. C. Swartzendruber, D. J. Kitko, P. W. Wertz, K. C. Madison, D. T. Downing, *Arch. Dermatol. Res.* **1988**, *280*, 424.
[32] T. Takeichi, T. Hirabayashi, Y. Miyasaka, A. Kawamoto, Y. Okuno, S. Taguchi, K. Tanahashi, C. Murase, H. Takama, K. Tanaka, W. E. Boeglin, M. W. Calcutt, D. Watanabe, M. Kono, Y. Muro, J. Ishikawa, T. Ohno, A. R. Brash, M. Akiyama, *J. Clin. Invest.* **2020**, *130*, 890.
[33] Y. Zheng, H. Yin, W. E. Boeglin, P. M. Elias, D. Crumrine, D. R. Beier, A. R. Brash, *J. Biol. Chem.* **2011**, *286*, 24046.
[34] L. E. Uche, G. S. Gooris, J. A. Bouwstra, C. M. Beddoes, *Biochim Biophys Acta Biomembr* **2021**, *1863*, 183487.
[35] S. Rebaud, O. Maniti, A. P. Girard-Egrot, *Biochimie* **2014**, *107 Pt A*, 135.
[36] D. J. McGillivray, G. Valincius, D. J. Vanderah, W. Febo-Ayala, J. T. Woodward, F. Heinrich, J. J. Kasianowicz, M. Losche, *Biointerphases* **2007**, *2*, 21.
[37] J. M. Meyer, D. Crumrine, H. Schneider, A. Dick, M. Schmuth, R. Gruber, F. P. W. Radner, S. Grond, J. S. Wakefield, T. M. Mauro, P. M. Elias, *Am. J. Pathol.* **2021**, *191*, 921.
[38] M. J. Sarmento, M. Prieto, F. Fernandes, *Biochim. Biophys. Acta* **2012**, *1818*, 2605.
[39] Y. Kitajima, T. Sekiya, S. Mori, Y. Nozawa, H. Yaoita, *J. Invest. Dermatol.* **1985**, *84*, 149.
[40] C. S. Poojari, K. C. Scherer, J. S. Hub, *Nat. Commun.* **2021**, *12*, 6594.
[41] M. E. Stewart, D. T. Downing, *J. Lipid Res.* **2001**, *42*, 1105.
[42] S. A. Akimov, V. A. Frolov, P. I. Kuzmin, J. Zimmerberg, Y. A. Chizmadzhev, F. S. Cohen, *Phys. Rev. E Stat. Nonlin. Soft Matter Phys.* **2008**, *77*, 051901.
[43] A. Mangiarotti, M. Siri, N. W. Tam, Z. Zhao, L. Malacrida, R. Dimova, *Nat. Commun.* **2023**, *14*, 6081.
[44] H. Y. Wang, S. H. Chan, S. Dey, I. Castello-Serrano, M. K. Rosen, J. A. Ditlev, K. R. Levental, I. Levental, *Sci. Adv.* **2023**, *9*, eadf6205.
[45] R. Rubio-Sanchez, B. M. Mognetti, P. Cicuta, L. Di Michele, *J. Am. Chem. Soc.* **2023**, *145*, 11265.
[46] C. Bernardini, S. D. Stoyanov, L. N. Arnaudov, M. A. Cohen Stuart, *Chem. Soc. Rev.* **2013**, *42*, 2100.
[47] M. L. Longo, A. M. Bisagno, J. A. Zasadzinski, R. Bruni, A. J. Waring, *Science* **1993**, *261*, 453.
[48] M. M. Lipp, K. Y. C. Lee, D. Y. Takamoto, J. A. Zasadzinski, A. J. Waring, *Phys. Rev. Lett.* **1998**, *81*, 1650.
[49] A. Novackova, I. Sagrafena, P. Pullmannova, G. Paraskevopoulos, A. Dwivedi, A. Mazumder, K. Ruzickova, P. Slepicka, J. Zbytovska, K. Vavrova, *J. Invest. Dermatol.* **2021**, *141*, 1915.
[50] B. Skolova, K. Hudska, P. Pullmannova, A. Kovacik, K. Palat, J. Roh, J. Fleddermann, I. Estrela-Lopis, K. Vavrova, *J. Phys. Chem. B* **2014**, *118*, 10460.
[51] L. Norlen, M. Lundborg, C. Wennberg, A. Narangifard, B. Daneholt, *J. Invest. Dermatol.* **2022**, *142*, 285.
[52] I. Iwai, H. Han, L. den Hollander, S. Svensson, L. G. Ofverstedt, J. Anwar, J. Brewer, M. Bloksgaard, A. Laloeuf, D. Nosek, S. Masich, L. A. Bagatolli, U. Skoglund, L. Norlen, *J. Invest. Dermatol.* **2012**, *132*, 2215.
[53] P. Jancalkova, M. Kopecna, M. Kurka, A. Kovacik, L. Opalka, I. Sagrafena, K. Vavrova, *J. Invest. Dermatol.* **2023**, *143*, 2427.
[54] D. Y. Takamoto, E. Aydil, J. A. Zasadzinski, A. T. Ivanova, D. K. Schwartz, T. Yang, P. S. Cremer, *Science* **2001**, *293*, 1292.
[55] L. Caseli, R. G. Oliveira, D. C. Masui, R. P. Furriel, F. A. Leone, B. Maggio, M. E. Zaniquelli, *Langmuir* **2005**, *21*, 4090.
[56] P. W. Wertz, K. C. Madison, D. T. Downing, *J. Invest. Dermatol.* **1989**, *92*, 109.
[57] P. Milani, J. Chlasta, R. Abdayem, S. Kezic, M. Haftek, *J. Mol. Recognit.* **2018**, *31*, 2722.
[58] J. B. Fournier, N. Khalifat, N. Puff, M. I. Angelova, *Phys. Rev. Lett.* **2009**, *102*, 018102.
[59] D. W. Thompson, *On Growth and Form*, Cambridge Univ. Press, Cambridge, **1917**.
[60] J. Steinkuhler, E. Sezgin, I. Urbancic, C. Eggeling, R. Dimova, *Commun Biol* **2019**, *2*, 337.
[61] N. F. Hadley, *Prog. Lipid Res.* **1989**, *28*, 1.
[62] N. F. Hadley, *Adv. Lipid Res.* **1991**, *24*, 303.
[63] L. Opalka, A. Kovacik, M. Sochorova, J. Roh, J. Kunes, J. Lenco, K. Vavrova, *Org. Lett.* **2015**, *17*, 5456.
[64] E. G. Bligh, W. J. Dyer, *Can. J. Biochem. Phys.* **1959**, *37*, 911.
[65] K. Vavrova, D. Henkes, K. Struver, M. Sochorova, B. Skolova, M. Y. Witting, W. Friess, S. Schreml, R. J. Meier, M. Schafer-Korting, J. W. Fluhr, S. Kuchler, *J. Invest. Dermatol.* **2014**, *134*, 746.
[66] P. Pullmannova, K. Stankova, M. Pospisilova, B. Skolova, J. Zbytovska, K. Vavrova, *Biochim. Biophys. Acta* **2014**, *1838*, 2115.
[67] P. J. Koch, P. A. de Viragh, E. Scharer, D. Bundman, M. A. Longley, J. Bickenbach, Y. Kawachi, Y. Suga, Z. Zhou, M. Huber, D. Hohl, T. Kartasova, M. Jarnik, A. C. Steven, D. R. Roop, *J. Cell Biol.* **2000**, *151*, 389.
[68] W. Abraham, D. T. Downing, *Biochim. Biophys. Acta* **1990**, *1021*, 119.
[69] T. Hirao, M. Denda, M. Takahashi, *Exp. Dermatol.* **2001**, *10*, 35.
[70] T. Hirao, T. Terui, I. Takeuchi, H. Kobayashi, M. Okada, M. Takashahi, H. Tagami, *Exp. Dermatol.* **2003**, *12*, 591.
[71] D. Groen, G. S. Gooris, J. A. Bouwstra, *Langmuir* **2010**, *26*, 4168.
[72] M. Sochorova, P. Audrlicka, M. Cervena, A. Kovacik, M. Kopecna, L. Opalka, P. Pullmannova, K. Vavrova, *J. Colloid. Interf Sci* **2019**, *535*, 227.
[73] B. Skolova, A. Kovacik, O. Tesar, L. Opalka, K. Vavrova, *Bba-Biomembranes* **2017**, *1859*, 824.